Extraordinary negative thermal expansion of two-dimensional nitrides: A comparative *ab initio* study of quasiharmonic approximation and molecular dynamics simulations

Ilker Demiroglu [1,*] and Cem Sevik [2,3,†]

[1]*Department of Advanced Technologies, Eskisehir Technical University, Eskisehir, TR 26555, Turkey*
[2]*Department of Physics, University of Antwerp, Groenenborgerlaan 171, 2020 Antwerp, Belgium*
[3]*Department of Mechanical Engineering, Eskişehir Technical University, Eskisehir, TR 26555, Turkey*

(Received 24 July 2020; accepted 27 January 2021; published 22 February 2021)

Thermal expansion behavior of two-dimensional (2D) nitrides and graphene were studied by *ab initio* molecular dynamics (MD) simulations as well as quasiharmonic approximation (QHA). Anharmonicity of the acoustic phonon modes are related to the unusual negative thermal expansion (NTE) behavior of the nitrides. Our results also hint that direct *ab initio* MD simulations are a more elaborate method to investigate thermal expansion behavior of 2D materials than the QHA. Nevertheless, giant NTE coefficients are found for *h*-GaN and *h*-AlN within the covered temperature range 100–600 K regardless of the chosen computational method. This unusual NTE of 2D nitrides is reasoned with the out-of-plane oscillations related to the rippling behavior of the monolayers.

DOI: 10.1103/PhysRevB.103.085430

I. INTRODUCTION

After the discovery of graphene [1] and such two-dimensional (2D) nanomaterials with extraordinary properties [2,3] that will help to miniaturize further technological devices with even higher efficiency than their predecessors, a route (forming heterostructures) emerged to mix and match the members of this materials family to further improve and adjust their properties [3,4]. In that sense, thermal properties of these nanomaterials are becoming even more critical for the performance, reliability, longevity, and safety of future device technology. Thermal expansion properties are particularly important because, at working temperatures, the accumulated thermal strain and stress may influence or even destroy the device performance.

Particularly, materials with negative thermal expansion (NTE) properties among the emerging 2D materials family are important, as compromising thermal expansion by NTE materials is a convenient way to eliminate the thermal expansion problems [5,6]. Very recently, it has been also shown that strain engineering via thermal expansion mismatch is an elaborate growth method for 2D materials [7], and it is shown that strain-engineered heterostructures exhibit superior ion battery performances [8]. To promote a wide range of device applications, it has been long desired to develop materials with larger NTE over a wide temperature range. On the other hand, even for bulk materials, only a limited number of NTE materials can serve as thermal expansion compensators in practice, due to the relatively narrow NTE operation-temperature window, low NTE coefficient, thermal expansion anisotropy, as well as low mechanical and/or electrical insulating properties [9]. However, because of a recent experiment, NTE behavior for monolayer to trilayer *h*-BN at 300 to 400 K temperatures is presented [10].

As the pioneer of 2D materials, the thermal expansion property of graphene has been studied more predominantly than other materials. Although NTE behavior is observed in general for lower temperatures, both experimental [11–18] and theoretical [19–33] results are very diverse and, in some cases, contradictory. For example, the experimental room temperature (RT) thermal expansion coefficients range from $-21.4 \times 10^{-6}\,\mathrm{K}^{-1}$ [11] to $-5.5 \times 10^{-6}\,\mathrm{K}^{-1}$ [12]. While some studies report a sharp increase [13,14] and a sign change to positive at around 350 K [13–15], others state more horizontal behavior and no sign change up to 1000 K [12,16]. In theoretical studies, on the other hand, thermal expansion values range from $-10 \times 10^{-6}\,\mathrm{K}^{-1}$ [19] to positive values [20] at RT, while they show different behaviors with respect to temperature due to the selected approach and the level of theory. This diversity is related to the importance of anharmonicities and rippling [34]. Moreover, even for the same method calculations within the conventional quasiharmonic approach, the RT values vary between $-3.5 \times 10^{-6}\,\mathrm{K}^{-1}$ [21] to $-1 \times 10^{-6}\,\mathrm{K}^{-1}$ [22], which is most probably due to the selected volume range and the existence of negative frequency phonons for the compressed models [23].

In general, direct experimental measurement of the thermal expansion coefficient of 2D materials is a rough task and usually dependent on simulations due to (I) the unwanted substrate effects, which usually dominate the thermal expansion behavior, and (II) the transparency of 2D materials, which makes conventional optical approaches difficult [35]. Therefore, accurate theoretical procedures for the determination of the thermal expansion coefficients of 2D materials are indispensable. As the NTE behavior typically originates from the presence of low-energy anharmonic vibrations of

*ilkerdemiroglu@eskisehir.edu.tr
†csevik@eskisehir.edu.tr

atoms [36], the quasiharmonic approach is likely to miss the full extent of the phenomenon. On the other hand, molecular dynamics (MD) is an elaborate method which incorporates full anharmonic interactions. However, its required large simulation system sizes to simulate thermal expansion behavior is usually a limiting factor for more accurate quantum level calculations, and therefore, it is studied more predominantly by various classical interaction potentials to date [20,31–33]. In this respect, we investigate thermal expansion coefficients of graphene *h*-BN, *h*-GaN, and *h*-AlN monolayers directly by *ab initio* MD simulations as well as the quasiharmonic approximation (QHA) and Grüneisen framework. To our knowledge, there is a lack of thermal expansion studies on monolayer GaN and AlN, apart from one QHA paper on *h*-GaN [37] showing NTE behavior only below RT with a maximum value of $-8 \times 10^{-6}\,\mathrm{K}^{-1}$ at 70 K.

II. METHODS

All simulations were performed by using density functional theory (DFT) within the Vienna *ab initio* Simulation Package (VASP) [38,39]. Local density approximation [40] and projector augmented wave [41,42] methods were used together with 500 eV plane-wave basis cutoff energy. For the vibrational frequency calculations, the plane-wave basis cutoff was increased to 700 eV. The vibrational frequencies were acquired by using the PHONOPY code [43], which can directly use the force constants obtained by density functional perturbation theory [44] provided by the VASP code. Here, $7 \times 7 \times 1$ conventional supercell structures and $5 \times 5 \times 1$ Γ centered *k*-points grids were considered for all systems. Isothermal-isobaric, NPT [45,46] ensemble have been selected for *ab initio* MD [47,48] simulations. We only applied the constant pressure algorithm to the two lattice vectors parallel to the 2D plane, leaving the third vector unchanged during the simulation. MD simulations were carried for a set of constant temperatures ranging from 50 to 600 K. At each temperature, all *ab initio* MD simulations lasted at least 8 ps with a time step of 1 fs. The friction coefficients of atomic and lattice degrees of freedom were set to $5\,\mathrm{ps}^{-1}$, and the external pressure was kept at 0 Pa.

III. RESULTS

To estimate the thermal expansion coefficient from QHA, all phonon frequencies of relaxed systems were calculated together with compressed and strained systems. Figure 1 shows phonon dispersion relations of graphene as an example. Although no negative frequencies exist for relaxed and strained configurations, imaginary frequencies exist for the first mode close to the Γ point in all the compressed configurations starting from 0.25% compression. As imaginary frequencies are not valid in QHA, we fitted vibrational frequencies of the compressed systems according to the linear relation obtained from the strained phonons. The fitted phonon frequencies correct the negative frequencies of the first mode, while the rest of the vibrational modes match very accurately with the existing ones. The same procedure was also applied to *h*-BN, *h*-AlN, and *h*-GaN systems, and similar results were obtained.

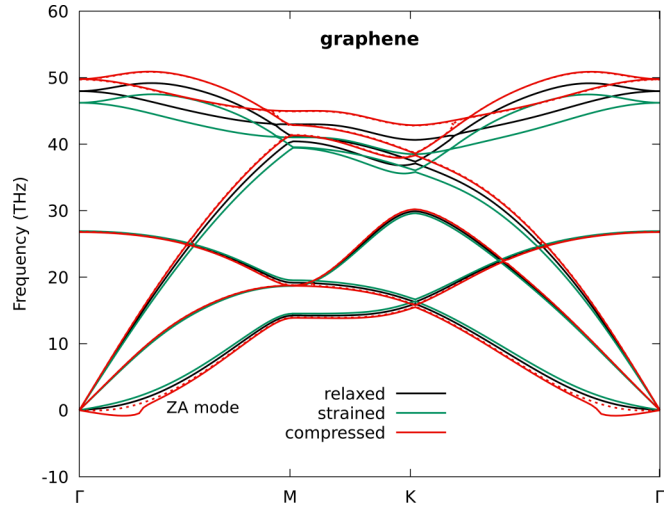

FIG. 1. Phonon dispersion relations of relaxed, 1% strained, and 1% compressed graphene monolayers. Dashed line shows the corrected phonon curves of the compressed case.

When noncorrected phonons, which have negative phonon frequencies, are used in QHA, thermal expansion values underestimate significantly. For *h*-GaN, the position of the minimum and the general shape matches well with the previous QHA paper [37]. For graphene and *h*-BN, thermal expansion values become positive at around 350 and 400 K, respectively, while for *h*-AlN and *h*-GaN, they become positive just before RT. On the other hand, with corrected phonons, thermal expansion values are negative for all systems in the covered temperature range 100–600 K. The NTE behavior is found to be giant for *h*-GaN and *h*-AlN, with similar values around $-20 \times 10^{-6}\,\mathrm{K}^{-1}$ at RT. For *h*-BN, it is estimated around $-10 \times 10^{-6}\,\mathrm{K}^{-1}$ at RT, while for graphene, it is around $-6 \times 10^{-6}\,\mathrm{K}^{-1}$.

Thermal expansion (α) can be also obtained by the Grüneisen framework approach by calculating mode-dependent Grüneisen parameters ($\gamma_{q,j}$)

$$\gamma_{q,j} = -\frac{a_0}{\omega_{q,j}} \frac{\partial \omega_{q,j}}{\partial a}, \tag{1}$$

and the mean Grüneisen parameter (γ_{mean})

$$\gamma_{\mathrm{mean}} \equiv \frac{\sum_{q,j} \gamma_{q,j} c_{q,j}}{\sum_{q,j} c_{q,j}}, \tag{2}$$

as

$$\alpha = \frac{\gamma_{\mathrm{mean}} C^V}{B_T V_0}\Big|_{a,T}, \tag{3}$$

where a_0 is the unit cell constant, $\omega_{q,j}$ is the vibrational frequency corresponding to wave vector q and mode j, $c_{q,j}$ is the mode specific heat, C^V is the heat capacity, and B_T is the bulk modulus. We calculated the thermal expansion coefficient by considering 0.25% strained systems as the phonon behavior deviates from linearity with the increasing strain. Figure 2 shows that the thermal expansion behavior from the Grüneisen framework and from corrected QHA are the same, while the

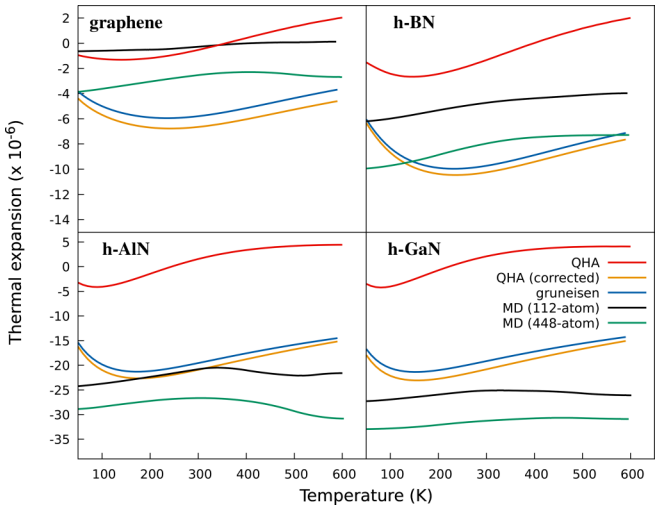

FIG. 2. Calculated thermal expansion coefficients of graphene and two-dimensional (2D) nitrides by molecular dynamics (MD) simulations, quasiharmonic approximation (QHA), and the Grüneisen framework.

absolute values of the Grüneisen framework are slightly larger than QHA in magnitude.

Strong anharmonicity of lattice vibrations are expected generally for 2D materials, and it is argued that anharmonicity is fundamental for their stability. In the case of graphene, for example, the anharmonic coupling between bending and stretching modes, which are decoupled in the harmonic approximation, can stabilize the flat phases by suppressing the long-wavelength fluctuations [27,34,49]. As given in Eq. (1), mode Grüneisen parameters are basically the strain dependence of phonon frequencies, and they are often used as a heuristic method to quantify anharmonicity. Mode Grüneisen parameters calculated over full mesh are given in Fig. 3 for

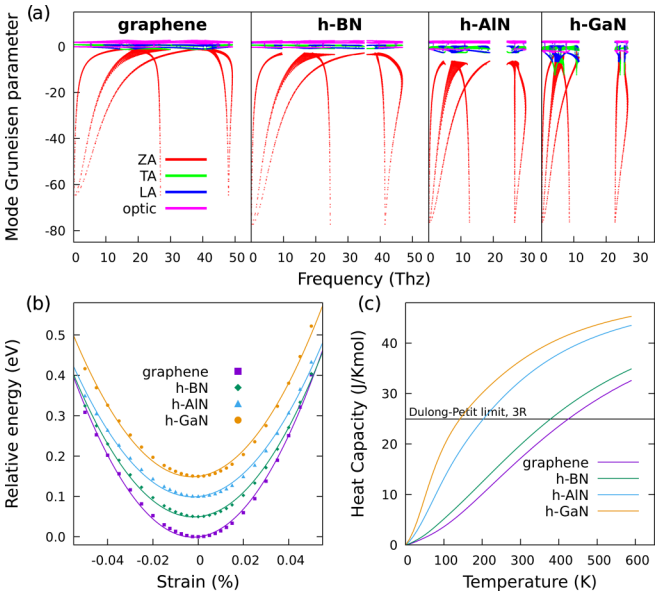

FIG. 3. Calculated (a) mode Grüneisen parameters, (b) energy vs strain curves, and (c) heat capacity vs temperature curves for graphene and two-dimensional (2D) nitrides.

all considered 2D systems. The ZA branch (the out-of-plane vibration) is the main negative contributor in all four systems, while the optic branches are condensed around 0. For *h*-AlN and especially for *h*-GaN, the other acoustic branches also start to contribute negative means, which indicate stronger anharmonicity for these materials, and it is also reflected in their stronger NTE behavior.

The potential energy change due to the strain can also hint at phonon anharmonicity from another point of view. Here, the strain is defined by the change of the lattice constant divided by its relaxed value, $[(a - a_0)/a_0]$. The potential energy wells (given in Fig. 3) obtained from strained and compressed systems with respect to the positive and negative atomic displacements were found strongly asymmetric and thus deviate from harmonic behavior. The cubic terms of the polynomial fitting quantify the order of the anharmonicity as -421, -357, -332, and -317 meV Å^{-3} for *h*-GaN, graphene, *h*-AlN, and *h*-BN, respectively. The values for *h*-GaN and graphene are in good agreement with the results of a previous paper [50]. This anharmonicity consideration is also in line with the MD simulations, where the bond length distribution around the equilibrium shows an asymmetry from harmonic behavior, and more states were found for larger distances than the smaller ones [see Fig. 4(a) in the next part as an example for *h*-GaN].

Another indication of the strong anharmonicity is the increase of specific heat beyond the Dulong-Petit limit (see Fig. 3 inset). The heat capacity values obtained from QHA exceed the Dulong-Petit limit, even before 200 K for *h*-GaN and *h*-AlN, and increase with the increasing temperature. The order is found as *h*-GaN > *h*-AlN > *h*-BN > graphene. The heat capacity values obtained from *ab initio* MD simulations, on the other hand, show a constant behavior within the temperature range (100–600 K), as in the case of a previous Monte Carlo paper on graphene [27], but sits above Dulong-Petit limit with similar values around 25.2 Jmol^{-1} K^{-1} for all four systems. All in all, the perceived anharmonicity order matches well with the order in thermal expansion coefficients in general, as the anharmonicity is the main driving force for the NTE behavior in 2D materials [36].

To include the full anharmonic effects into the consideration of the thermal expansion behavior, *ab initio* MD simulations were conducted directly at DFT level. As the rippling effects are important in the NTE behavior of 2D materials, the size of the system under the periodic boundary conditions becomes significant and should be treated carefully. Thus, also considering the limits of the DFT-type quantum mechanical calculations, we constructed four different system sizes containing 112, 240, 336, and 448 atoms inside rectangular unit cells in the *xy* plane. The most drastic difference was found for the graphene system; for the smallest system size, the area of the cell almost does not change with increasing temperature and therefore underestimates the thermal expansion significantly (see Fig. 5). For 2D nitrides, differences are smaller, and the results seem to converge as the system size increases up to 448 atoms (see Fig. 5). The normalized area values decrease for each material with the increasing temperature, as expected, and the decreased order in magnitude follows the same anharmonicity order between the four considered materials: *h*-GaN > *h*-AlN > *h*-BN >

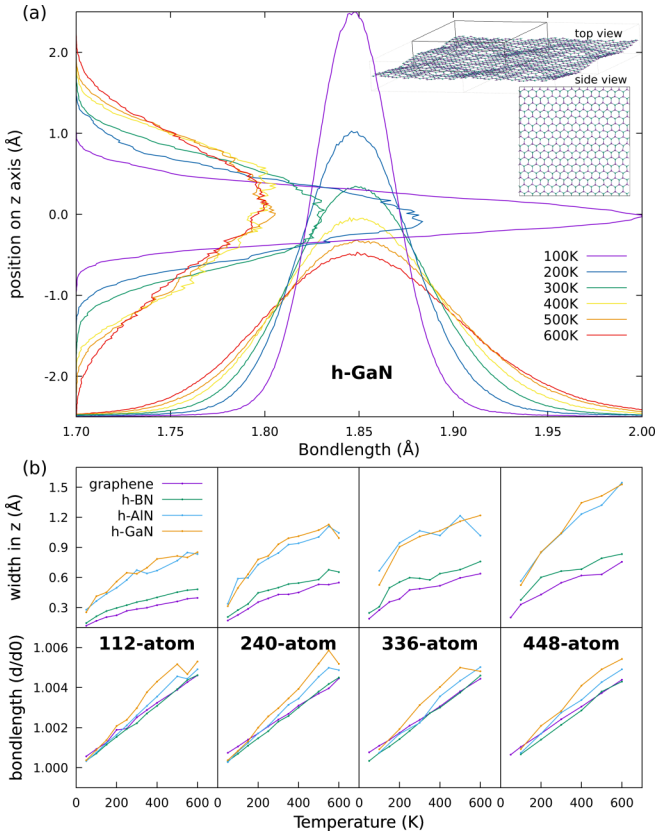

FIG. 4. (a) Statistical structural analysis of 448-atom *h*-GaN obtained from molecular dynamics (MD) simulations. The bond length distribution is given in the horizontal axis, while the position distribution on the z axis is given in the vertical axis. Insets show the top and side views of a MD timeframe. (b) Normalized bond lengths vs temperature and rippling width vs temperature graphs of graphene and two-dimensional (2D) nitrides obtained from MD simulations.

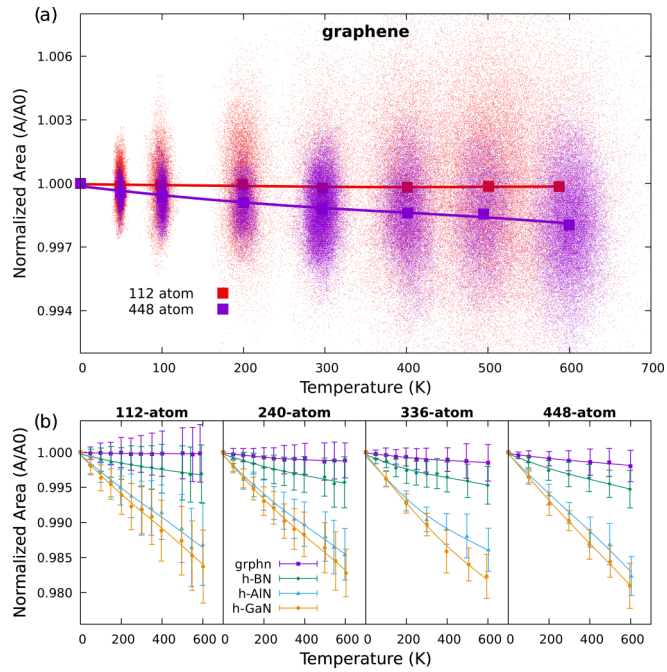

FIG. 5. Normalized area vs simulation temperature for molecular dynamics (MD) calculations. (a) The data values of each MD frame are shown in the top graph, while (b) the standard deviation is given in the bottom graphs for each size.

graphene. However, the radial distribution function analyses show that the bond lengths increase linearly with the increasing temperature for each system, and they seem independent from the system size. On the other hand, variation of the atom positions on the z axis is affected by the system size, as the smaller unit cells do not allow the full extent of the rippling behavior (do not excite long wavelength out-of-plane vibrations, particularly in the ZA mode). Therefore, the calculated thermal expansion coefficients were always found lower in magnitude for smaller system sizes. Figure 4 shows explicitly how the bond lengths and the rippling behaviors change with respect to temperature in the 448-atom *h*-GaN system, and the information for the other system sizes and other materials are given in terms of rippling width (width in the z axis) and normalized bond lengths ($\frac{d_T}{d_0}$). These results clearly depict that the observed decrease in the area is solely due to the rippling effects, which are the result of out-of-plane vibrations (ZA mode).

The rippling behavior was found largest for *h*-GaN and *h*-AlN, which causes the giant NTE behavior for these 2D materials. In general, the order of the rippling behavior also follows the order of the thermal expansion behavior: *h*-GaN $>$ *h*-AlN $>$ *h*-BN $>$ graphene. Previous papers have also reported that the NTE behavior in graphene is mainly from rippling, and this paper confirms that this behavior is general for 2D nitrides. Thermal expansion values around RT are found as -31×10^{-6}, -27×10^{-6}, -7×10^{-6}, and $-2.5 \times 10^{-6}\,\mathrm{K}^{-1}$ for *h*-GaN, *h*-AlN, *h*-BN, and graphene, respectively, from the *ab initio* MD simulations by taking the base as the largest 448-atom systems. The RT thermal expansion value of $-7 \times 10^{-6}\,\mathrm{K}^{-1}$ for *h*-BN is also in good agreement with the results of the path integral of Monte Carlo and self-consistent phonon method calculations, which consider nuclear quantum effects, by Calvo *et al.* [51]. One should note that the NTE values of *h*-GaN and *h*-AlN are gigantic, which deserves scientific interest, as giant NTE materials are rare and could be taken advantage of from a technological point of view. Thus, experimental confirmation of the giant NTE behavior of *h*-GaN and *h*-AlN should take precedence in 2D materials research.

When we compare the thermal expansion values obtained from the MD simulations with those from QHA, it can be seen that the NTE behavior is overestimated by QHA in the cases for graphene and *h*-BN and underestimated for *h*-AlN and *h*-GaN. Thus, the absolute differences between QHA and MD methods hint at a reverse trend for the thermal expansion behavior with respect to the anharmonicity order. This trend is also in line with the expected trend of stronger NTE behavior for 2D materials with increasing anharmonicity, which hints that the MD method captures the phenomenon more completely than QHA in terms of anharmonicity. When we compare our thermal expansion values for *h*-BN with another theoretical paper [51] involving nuclear quantum effects, we can conclude that MD results are in quite good agreement.

IV. CONCLUSIONS

To sum up, in this paper, we investigated the NTE behavior of graphene and 2D nitrides by *ab initio* MD and QHA methods. Our results clearly demonstrate that, regardless of the calculation method, *h*-GaN and *h*-AlN have giant NTE coefficients, while the *h*-BN system has also much larger NTE behavior than graphene. The anharmonicity considerations were found consistent with the NTE behavior, and the main contribution was found from the low-energy acoustic phonons. Statistical analysis from the *ab initio* MD simulations reveal that the bond length increases by the temperature for all the temperature ranges considered, and thus, the NTE behavior for 2D nitrides is solely from the rippling behavior structurally.

ACKNOWLEDGMENTS

Computational resources were provided by the High Performance and Grid Computing Center (TRGrid e-Infrastructure) of TUBITAK ULAKBIM and the National Center for High Performance Computing (UHeM) of Istanbul Technical University.

[1] K. S. Novoselov, A. K. Geim, S. V Morozov, D. Jiang, Y. Zhang, S. V Dubonos, I. V Grigorieva, and A. A. Firsov, Science **306**, 666 (2004).
[2] R. Mas-Ballesté, C. Gómez-Navarro, J. Gómez-Herrero, and F. Zamora, Nanoscale **3**, 20 (2011).
[3] K. S. Novoselov, A. Mishchenko, A. Carvalho, and A. H. Castro Neto, Science **353**, aac9439 (2016).
[4] A. K. Geim and I. V. Grigorieva, Nature **499**, 419 (2013).
[5] K. Takenaka, Sci. Technol. Adv. Mater. **13**, 013001 (2012).
[6] Q. Wang, J. A. Jackson, Q. Ge, J. B. Hopkins, C. M. Spadaccini, and N. X. Fang, Phys. Rev. Lett. **117**, 175901 (2016).
[7] G. H. Ahn, M. Amani, H. Rasool, D. H. Lien, J. P. Mastandrea, J. W. Ager, M. Dubey, D. C. Chrzan, A. M. Minor, and A. Javey, Nat. Commun. **8**, 608 (2017).
[8] P. Xiong, F. Zhang, X. Zhang, S. Wang, H. Liu, B. Sun, J. Zhang, Y. Sun, R. Ma, Y. Bando, C. Zhou, Z. Liu, T. Sasaki, and G. Wang, Nat. Commun. **11**, 3297 (2020).
[9] Y. Nakamura, K. Takenaka, A. Kishimoto, and H. Takagi, J. Am. Ceram. Soc. **92**, 2999 (2009).
[10] Q. Cai, D. Scullion, W. Gan, A. Falin, S. Zhang, K. Watanabe, T. Taniguchi, Y. Chen, E. J. G. Santos, and L. H. Li, Sci. Adv. **5**, eaav0129 (2019).
[11] X. Hu, P. Yasaei, J. Jokisaari, S. Öğüt, A. Salehi-Khojin, and R. F. Klie, Phys. Rev. Lett. **120**, 055902 (2018).
[12] W. Pan, J. Xiao, J. Zhu, C. Yu, G. Zhang, Z. Ni, K. Watanabe, T. Taniguchi, Y. Shi, and X. Wang, Sci. Rep. **2**, 893 (2012).
[13] C. Li, Q. Liu, X. Peng, and S. Fan, Meas. Sci. Technol. **27**, 075102 (2016).
[14] W. Bao, F. Miao, Z. Chen, H. Zhang, W. Jang, C. Dames, and C. N. Lau, Nat. Nanotechnol. **4**, 562 (2009).
[15] S. Linas, Y. Magnin, B. Poinsot, O. Boisron, G. D. Förster, V. Martinez, R. Fulcrand, F. Tournus, V. Dupuis, F. Rabilloud, L. Bardotti, Z. Han, D. Kalita, V. Bouchiat, and F. Calvo, Phys. Rev. B **91**, 075426 (2015).
[16] D. Yoon, Y. W. Son, and H. Cheong, Nano Lett. **11**, 3227 (2011).
[17] G. López-Polín, M. Ortega, J. G. Vilhena, I. Alda, J. Gomez-Herrero, P. A. Serena, C. Gomez-Navarro, and R. Pérez, Carbon **116**, 670 (2017).
[18] V. Singh, S. Sengupta, H. S. Solanki, R. Dhall, A. Allain, S. Dhara, P. Pant, and M. M. Deshmukh, Nanotechnology **21**, 165204 (2010).
[19] V. N. Bondarev, V. M. Adamyan, and V. V. Zavalniuk, Phys. Rev. B **97**, 035426 (2018).
[20] H. Ghasemi and A. Rajabpour, J. Phys. Conf. Ser. **785**, 012006 (2017).
[21] N. Mounet and N. Marzari, Phys. Rev. B **71**, 205214 (2005).
[22] T. Shao, B. Wen, R. Melnik, S. Yao, Y. Kawazoe, and Y. Tian, J. Chem. Phys. **137**, 194901 (2012).
[23] X. J. Ge, K. L. Yao, and J. T. Lü, Phys. Rev. B **94**, 165433 (2016).
[24] S. Mann, P. Rani, R. Kumar, and V. K. Jindal, AIP Conf. Proc. **1731**, 110038 (2016).
[25] S. Mann, R. Kumar, and V. K. Jindal, RSC Adv. **7**, 22378 (2017).
[26] C. Sevik, Phys. Rev. B **89**, 035422 (2014).
[27] K. V. Zakharchenko, M. I. Katsnelson, and A. Fasolino, Phys. Rev. Lett. **102**, 046808 (2009).
[28] J. W. Jiang, J. S. Wang, and B. Li, Phys. Rev. B **80**, 205429 (2009).
[29] E. Madenci, A. Barut, and M. Dorduncu, in *2019 IEEE 69th Electronic Components and Technology Conference (ECTC)* (Institute of Electrical and Electronics Engineers Inc., Las Vegas, 2019), pp. 825–833.
[30] M. Pozzo, D. Alfè, P. Lacovig, P. Hofmann, S. Lizzit, and A. Baraldi, Phys. Rev. Lett. **106**, 135501 (2011).
[31] W. Gao and R. Huang, J. Mech. Phys. Solids **66**, 42 (2014).
[32] Alamusi, H. Li, Y. Ning, B. Gu, N. Hu, W. Yuan, F. Jia, H. Liu, Y. Li, Y. Liu, H. Ning, L. Wu, S. Fu, and Y. Cai, Mol. Simul. **44**, 34 (2018).
[33] C. P. Herrero and R. Ramírez, J. Chem. Phys. **148**, 102302 (2018).
[34] A. Fasolino, J. H. Los, and M. I. Katsnelson, Nat. Mater. **6**, 858 (2007).
[35] L. Zhang, Z. Lu, Y. Song, L. Zhao, B. Bhatia, K. R. Bagnall, and E. N. Wang, Nano Lett. **19**, 4745 (2019).
[36] R. Mittal, M. K. Gupta, and S. L. Chaplot, Prog. Mater. Sci. **92**, 360 (2018).
[37] G. Qin, Z. Qin, H. Wang, and M. Hu, Phys. Rev. B **95**, 195416 (2017).
[38] G. Kresse and J. Hafner, Phys. Rev. B **47**, 558 (1993).
[39] G. Kresse and J. Hafner, Phys. Rev. B **49**, 14251 (1994).
[40] J. P. Perdew and A. Zunger, Phys. Rev. B **23**, 5048 (1981).
[41] G. Kresse and D. Joubert, Phys. Rev. B **59**, 1758 (1999).
[42] P. E. Blöchl, Phys. Rev. B **50**, 17953 (1994).
[43] A. Togo, F. Oba, and I. Tanaka, Phys. Rev. B **78**, 134106 (2008).
[44] S. Baroni, S. De Gironcoli, A. Dal Corso, and P. Giannozzi, Rev. Mod. Phys. **73**, 515 (2001).

[45] E. Hernández, J. Chem. Phys. **115**, 10282 (2001).
[46] M. P. Allen and D. J. Tildesley, *Computer Simulation of Liquids*, Second Edition (Oxford University Press, Oxford, 2017).
[47] M. Parrinello and A. Rahman, J. Appl. Phys. **52**, 7182 (1981).
[48] M. Parrinello and A. Rahman, Phys. Rev. Lett. **45**, 1196 (1980).
[49] A. L. C. Da Silva, L. Cândido, J. N. Teixeira Rabelo, G. Q. Hai, and F. M. Peeters, Europhys. Lett. **107**, 56004 (2014).
[50] Z. Qin, G. Qin, X. Zuo, Z. Xiong, and M. Hu, Nanoscale **9**, 4295 (2017).
[51] F. Calvo and Y. Magnin, Eur. Phys. J. B **89**, 56 (2016).